
Mitigating State Aliasing in Vision-Language-Action Models via Inverse Dynamics Learning

| | | |
|--|---|--|
| Kyu Jin Lee KAIST kyujinlee@kaist.ac.kr | Injae Kim KAIST injae.kim@kaist.ac.kr | Jihwan Park KAIST jseven7071@kaist.ac.kr |
| Yejun Ju KAIST dpwns99@kaist.ac.kr | Minseok Joo Korea University wlgkcjf87@korea.ac.kr | Hyunwoo J. Kim* KAIST hyunwoojkim@kaist.ac.kr |

Abstract

Vision-Language-Action (VLA) models have emerged as a promising framework that unifies perception, reasoning, and control for handling robot manipulation tasks by adapting pretrained vision-language models (VLMs) to action prediction. However, VLM-derived representations are often insensitive to subtle visual distinctions required for low-level control, causing *state aliasing* between visually similar states but substantially different in required actions. Prior VLA studies improve visual understanding by training models to generate visual or reasoning outputs, such as future frames, 2D grounding points or traces, or intermediate spatial reasoning steps, but these objectives typically shape the vision encoder only indirectly through end-to-end output prediction, and state aliasing is not explicitly analyzed in the learned visual feature space. To mitigate state aliasing, we introduce **inverse dynamics learning** as an auxiliary objective that directly supervises the VLA vision encoder. By predicting the action between current and future observations, our objective encourages the encoder to capture fine-grained visual distinctions that determine the required low-level actions. We further use pseudo-reversed supervision to expose the encoder to a broader range of action directions and improve generalization under limited robot demonstrations. Our method is readily applicable to diverse VLA baselines, as it uses only observation-action pairs from standard manipulation datasets without additional annotations during training and preserves the original inference pipeline at test time. Experiments on CALVIN ABC \rightarrow D and SimplerEnv demonstrate consistent performance gains across diverse VLA baselines. We further demonstrate, through frozen-encoder probing and state-feature alignment analyses, that our method learns state-discriminative visual representations that reduce state aliasing and better align with robot state changes.

1 Introduction

Vision-Language-Action (VLA) models have emerged as a promising framework for robot manipulation, as they map visual observations and language instructions to executable robot actions while leveraging the semantic priors of pretrained vision-language models (VLMs) [1, 2, 3, 4]. Despite this promise, robotic manipulation requires visual representations that go beyond high-level vision-language understanding. A policy must distinguish fine-grained state variations, such as the end-effector pose, object pose, and their spatial relation, which may be visually subtle but determine

*Corresponding author.

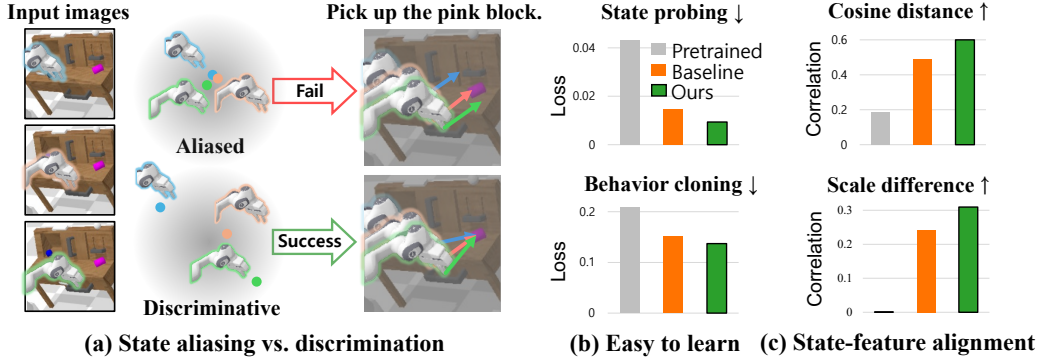


Figure 1: **Motivation and representation analysis.** (a) State aliasing maps visually similar states requiring different actions to nearby representations, causing ambiguous action prediction; state-discriminative representations instead separate relevant states and preserve meaningful robot-state structure. (b) Lower frozen-probe training loss indicates easier behavior and state prediction from the learned features, consistent with reduced state aliasing. (c) Higher structured state alignment suggests that our visual representations distinguish robot states while preserving their underlying state-space structure. Details are provided in Secs. 4.4 and 4.5.

the correct low-level action. Because VLM-derived representations are initially optimized for large-scale vision-language understanding, they primarily capture high-level semantic concepts and are insensitive to fine-grained spatial distinctions required for low-level control [5, 6, 7]. This can lead to **state aliasing** Fig. 1 (a), where visually similar but distinct states are mapped to insufficiently discriminative features, causing ambiguous action prediction. This motivates learning **state-discriminative visual representations** for reliable VLA policies.

Prior VLA studies have improved visual understanding for manipulation by training models to generate additional visual or reasoning targets, including visual prediction [8, 9, 10, 11, 12], 2D grounding [13, 14, 15, 16, 17, 18], and spatial reasoning before action prediction [19, 20, 21]. These decoding-oriented objectives provide useful supervision for the overall policy, but they are typically optimized end-to-end through output generation, leaving the vision encoder only indirectly supervised. Consequently, state aliasing remains underexplored: the encoder is not primarily trained or analyzed to distinguish visually similar states that require different actions.

To mitigate state aliasing in VLA policies, we introduce **inverse dynamics learning** as an auxiliary objective that directly supervises the vision encoder during training. Given current and future observations from a demonstration trajectory, the vision encoder independently extracts their visual features, and a lightweight inverse dynamics head predicts the intermediate action. This supervision encourages the encoder to retain action-grounded visual distinctions that determine low-level actions, making visually similar states that require different actions more separable in the feature space. As shown in Fig. 1 (b), compared with standard VLA training, our objective yields visual representations from which downstream policies can learn more easily, suggesting reduced state aliasing. Moreover, in Fig. 1 (c), the feature space is not merely more separable, but also better aligned with actual robot state changes. These representation gains are obtained with an auxiliary head that is used only during training and removed afterward, leaving the original VLA architecture and inference process intact.

To further strengthen the inverse dynamics learning, we introduce **Pseudo Time Reversal (PTR)**, an augmentation for inverse dynamics learning that addresses the one-directional nature of robot demonstrations. Because robot datasets typically contain only actions along successful trajectories, the model sees limited action variation around similar visual states. This can encourage the vision encoder to rely on coarse directional shortcuts, such as trajectory direction or task progress, rather than action-relevant fine-grained visual distinctions, weakening generalization beyond the demonstrated action patterns [22, 23, 24]. PTR constructs pseudo-reversed supervision from the same demonstrations by temporally reversing the observation order and pairing it with pseudo-ground-truth reversed actions. This exposes the encoder to both forward and pseudo-reversed action directions, expanding action diversity and reducing reliance on directional shortcuts in vision encoder learning.

Extensive experiments on CALVIN ABC→D [25] and SimplerEnv [26] show that our method consistently improves end-to-end policy performance across diverse VLA baselines. Frozen-encoder evaluations on LIBERO [27] further show that the learned representations support easier downstream action and robot state prediction, while state-feature alignment analysis demonstrates stronger correspondence between visual feature distances and ground-truth robot state changes. Together, these results indicate that our method mitigates state aliasing by learning visual features that are both more separable and more aligned with robot state geometry.

In summary, our contributions are threefold:

- We introduce a simple yet effective pretext task, inverse dynamics learning, that predicts actions between visual observations, encouraging a vision encoder in VLA to learn action-aware visual representations that mitigate state aliasing.
- We propose Pseudo Time Reversal (PTR), a data augmentation method that temporally reverses visual observations along with pseudo-ground-truth actions for more robust generalization under limited action diversity in low-demonstration regimes.
- Our experiments demonstrate that the proposed method provides consistent performance gains across diverse VLA baselines. The effectiveness of learned representations is also validated through frozen-encoder probing and state-feature alignment analysis.

2 Related Work

2.1 Vision-language-action models

Vision-language-action (VLA) models adapt pretrained vision-language models (VLMs) [1, 2, 3, 4] to map visual observations and language instructions to low-level robot actions, establishing VLM initialization as a central design choice for generalist robot policies [28, 29, 30, 14]. Recent studies have explored diverse policy formulations, including autoregressive token prediction [28, 30, 12], continuous action prediction via direct regression, diffusion, or flow matching [29, 31, 32], spatially grounded action prediction [33, 34], and hybrid discrete-continuous action modeling [35, 36]. Another line of work improves VLM-to-VLA adaptation through fine-tuning strategies, lightweight adapters, and compact policy architectures [37, 38, 39, 40].

2.2 Visual and reasoning supervision in VLA

Beyond policy architectures, recent work has explored supervision for visual understanding in VLA models. One line augments action learning with visual prediction objectives, such as future-frame or depth prediction, to provide spatial and temporal supervision beyond action prediction [8, 28, 10, 9, 11]. Another introduces grounding and reasoning objectives that anchor action prediction to fine-grained visual evidence or intermediate plans, including pixel- and trace-level supervision over task-relevant regions [13, 17, 14] and chain-of-thought, latent, or grounded reasoning prior to action [19, 21, 41, 20, 42, 43, 44]. Robot-state-aware contrastive learning has also been used to align VLA representations with proprioceptive states [45]. Although these approaches provide useful supervision, they are typically optimized through generated visual or reasoning outputs, leaving the vision encoder only indirectly supervised. In contrast, our method applies inverse dynamics supervision to the vision encoder itself to address state aliasing in the learned visual features.

2.3 Inverse dynamics modeling

Inverse dynamics predicts the action between two observations and has been used in several learning-based robotics settings. In predictive policy learning, it maps predicted future visual states to executable actions [46, 47, 48, 49]. Another line of work uses inverse dynamics to recover actions or latent actions from action-free videos, enabling policy learning without explicit action labels [50, 51, 52, 53]. Closest to our work, inverse dynamics has been studied for imitation learning and visual representation learning, where predicting actions from state transitions helps preserve control-relevant information [54, 55, 56, 57]. We adapt this idea for VLA vision encoder learning and introduce PTR to regularize representations under limited vision-action diversity.

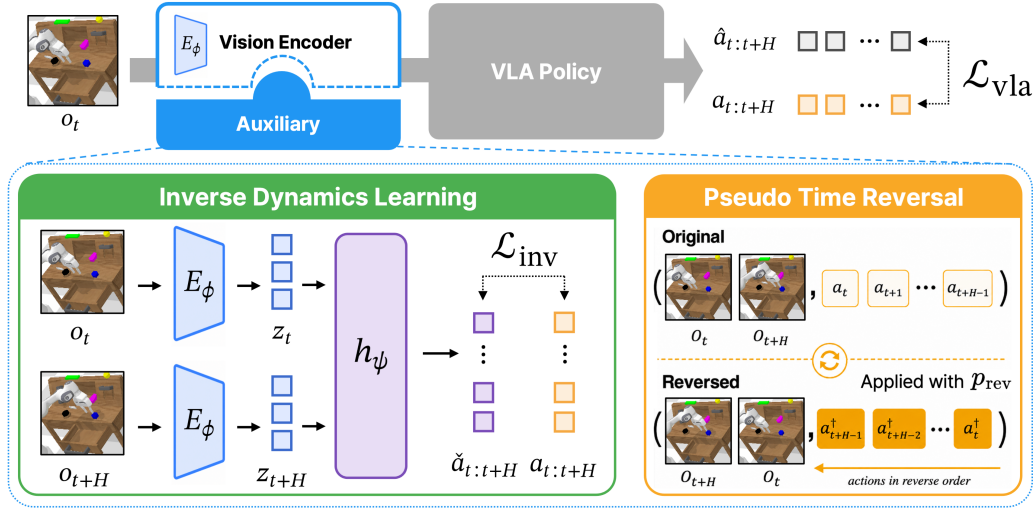


Figure 2: **Method overview.** To mitigate state aliasing in VLA policies, we supervise the vision encoder with inverse dynamics learning during training. In addition to the main VLA objective, the vision encoder E_ϕ independently encodes current and future observations (o_t, o_{t+H}) , and the inverse dynamics head h_ψ predicts the intermediate action sequence. This auxiliary supervision encourages the encoder to retain visual distinctions that determine low-level actions. PTR further constructs pseudo-reversed supervision by swapping the observation order and reversing the action sequence with negated motion offsets, improving generalization under limited action diversity. After training, the auxiliary head is removed, leaving the original VLA architecture and inference process intact.

3 Method

We propose inverse dynamics learning as an auxiliary objective that directly supervises the vision encoder to mitigate state aliasing. Our method encourages state-discriminative visual representation learning while keeping the main policy intact. We further introduce Pseudo Time Reversal (PTR) to improve generalization under limited action diversity in robot demonstrations. Sec. 3.1 presents the inverse dynamics objective, Sec. 3.2 introduces PTR, and Sec. 3.3 describes their integration with the main VLA objective.

3.1 Auxiliary inverse dynamics learning

Inverse dynamics is the task of predicting the action between two observations. We use this task as an auxiliary supervision signal for the VLA vision encoder, encouraging it to preserve visual differences that determine low-level robot actions.

We consider a language-conditioned robot manipulation dataset $\mathcal{D} = \{\tau_i\}_{i=1}^N$ consisting of demonstration trajectories. For a trajectory $\tau \in \mathcal{D}$, we write

$$\tau = (l, \{(o_t, a_t)\}_{t=1}^T),$$

where l denotes a language instruction, o_t denotes the visual observation at time step t , and a_t denotes the corresponding low-level robot action. Here, o_t may consist of one or more camera views. While the action space can vary across embodiments, we consider a 7-DoF single-gripper action space in this work:

$$a_t = [\Delta x_t, \Delta y_t, \Delta z_t, \Delta \phi_t, \Delta \theta_t, \Delta \psi_t, g_t],$$

where $\Delta x_t, \Delta y_t, \Delta z_t$ denote the relative translation offsets of the end-effector, $\Delta \phi_t, \Delta \theta_t, \Delta \psi_t$ denote the relative rotation offsets, and g_t denotes the gripper open/close action.

For an action chunk of length k , we use the notation

$$a_{t:t+k} = (a_t, a_{t+1}, \dots, a_{t+k-1}).$$

Given an observation pair (o_t, o_{t+k}) and the corresponding action chunk $a_{t:t+k}$, the vision encoder E_ϕ independently encodes the two observations into visual features z_t and z_{t+k} :

$$z_t = E_\phi(o_t), \quad z_{t+k} = E_\phi(o_{t+k}).$$

A lightweight inverse dynamics head h_ψ then predicts the intermediate action chunk:

$$\check{a}_{t:t+k} = h_\psi(z_t, z_{t+k}),$$

where $\check{a}_{t:t+k}$ denotes the inverse dynamics prediction.

We supervise this prediction with an auxiliary inverse dynamics loss:

$$\mathcal{L}_{\text{inv}} = \mathcal{L}_{\text{motion}}(\check{a}_{t:t+k}, a_{t:t+k}) + \lambda_g \mathcal{L}_{\text{grripper}}(\check{a}_{t:t+k}, a_{t:t+k}).$$

Here, $\mathcal{L}_{\text{motion}}$ is an ℓ_1 loss applied to the six end-effector motion offsets, $\mathcal{L}_{\text{grripper}}$ is a binary cross-entropy loss applied to the gripper action, and λ_g balances the two terms.

Since the auxiliary pairs are constructed directly from observation-action sequences already available in standard robot manipulation datasets, inverse dynamics learning requires no additional annotations while providing supervision that helps mitigate state aliasing in the vision encoder.

3.2 Pseudo Time Reversal

Robot manipulation datasets typically provide supervision only along successful forward trajectories. As a result, for a given image-language condition, the available actions often cover limited directional variation, which can encourage the vision encoder to rely on coarse directional patterns or task-irrelevant visual shortcuts rather than manipulation-relevant cues [24]. To mitigate this bias, we introduce Pseudo Time Reversal (PTR), a simple stochastic augmentation for auxiliary inverse dynamics learning.

Given an inverse dynamics sample $(o_t, o_{t+k}, a_{t:t+k})$, PTR constructs a pseudo-reversed sample by swapping the observation order and reversing the action sequence after negating its motion offsets. For each action a_i , we define

$$a_i^\dagger = [-\Delta x_i, -\Delta y_i, -\Delta z_i, -\Delta \phi_i, -\Delta \theta_i, -\Delta \psi_i, g_i].$$

Correspondingly, the pseudo-reversed counterpart of the action chunk $a_{t:t+k}$ is defined as

$$a_{t+k:t}^\dagger = (a_{t+k-1}^\dagger, a_{t+k-2}^\dagger, \dots, a_t^\dagger).$$

PTR is applied to each auxiliary sample with probability p_{rev} . The sample is kept as $(o_t, o_{t+k}, a_{t:t+k})$ with probability $1 - p_{\text{rev}}$, and converted to $(o_{t+k}, o_t, a_{t+k:t}^\dagger)$ with probability p_{rev} . This exposes the inverse dynamics objective to both forward and pseudo-reversed supervision.

The reversal is pseudo because negating the motion offsets produces motion in the opposite direction with respect to the original observation, rather than the physically exact action that returns from o_{t+H} to o_t . Since PTR is used only as an auxiliary signal, not as a target for the main VLA policy, this local approximation is sufficient to regularize visual representation learning without requiring reversed demonstrations.

3.3 Overall pipeline

We now describe how auxiliary inverse dynamics learning and PTR are integrated into standard VLA training. Let π_θ denote a VLA policy that predicts an action chunk $\hat{a}_{t:t+H}$ of length H from the current observation o_t and language instruction l :

$$\hat{a}_{t:t+H} = \pi_\theta(o_t, l).$$

The policy is trained with its original action prediction objective:

$$\mathcal{L}_{\text{vla}} = \ell(\hat{a}_{t:t+H}, a_{t:t+H}),$$

where ℓ denotes the model-specific action prediction loss.

For the auxiliary inverse dynamics objective, we use the same action chunk as the VLA target by setting $k = H$. Thus, each VLA training sample $(l, o_t, a_{t:t+H})$ is augmented with the future

observation o_{t+H} from the same trajectory to form an inverse dynamics sample $(o_t, o_{t+H}, a_{t:t+H})$. This auxiliary sample is then stochastically kept in its forward form or converted into its pseudo-reversed form with probability p_{rev} , as described in Sec. 3.2.

Using either the forward sample or its pseudo-reversed variant, we compute the auxiliary inverse dynamics loss \mathcal{L}_{inv} defined in Sec. 3.1. The overall training objective is

$$\mathcal{L} = \mathcal{L}_{\text{vla}} + \lambda_{\text{inv}} \mathcal{L}_{\text{inv}},$$

where λ_{inv} controls the strength of the auxiliary supervision.

Importantly, our method does not modify the policy architecture or its action prediction objective. The inverse dynamics head is attached only during training to provide additional supervision to the vision encoder, and is removed after training. At inference time, the original VLA policy π_{θ} is used intact, taking only the current observation and language instruction as input.

4 Experiments

We evaluate our method from two perspectives: end-to-end policy performance across various VLA architectures and whether the learned vision encoder reduces state aliasing in its visual representations. For policy evaluation, we benchmark our method on CALVIN ABC→D [25] and SimplerEnv (WidowX) [26] using multiple VLA baselines with different modeling choices. For representation analysis, we conduct frozen-encoder evaluations on LIBERO [27], comparing the original Qwen3VL-8B [4] vision encoder, VLM4VLA [58] after LIBERO-90 pretraining, and VLM4VLA + Ours. These evaluations test whether the learned visual features make downstream action and robot state prediction easier, which serves as evidence of reduced state aliasing. We further analyze state-feature alignment to examine whether visual feature distances better reflect robot-state changes, rather than merely separating observations. Finally, we include an ablation study to analyze the contribution of PTR.

4.1 Experimental setup

Baseline models. We compare our method against representative VLA baselines with different architectures and action modeling strategies. **VLM4VLA** [58] is a simple VLA framework built from a pretrained VLM with minimal architectural modification, predicting continuous actions via direct regression. **FLOWER** [39] is an efficient flow-based VLA model with a compact architecture and competitive action modeling performance. **SpatialVLA** [33] predicts actions through explicit 3D spatial modeling, allowing us to evaluate our method under a different inference structure.

For each benchmark, we compare each baseline with its +Ours variant: VLM4VLA and FLOWER on CALVIN ABC→D, and SpatialVLA on SimplerEnv. For LIBERO representation analysis, we compare Qwen3VL-8B, VLM4VLA, and VLM4VLA + Ours in the frozen-encoder setting.

Training protocol. For each baseline, we keep the original training pipeline unchanged and add only auxiliary inverse dynamics learning and PTR to supervise the vision encoder. To ensure a fair comparison, each baseline and its +Ours variant are trained under matched training budgets, hyperparameters, checkpoint selection rules, and evaluation protocols. We follow released configurations when available, use default implementation values for unspecified details, and report final-checkpoint performance. The auxiliary loss weight is tuned separately for each baseline. Detailed hyperparameters and benchmark-specific training budgets are provided in Appendix A.

4.2 CALVIN ABC→D

We evaluate our method on CALVIN ABC→D, a language-conditioned long-horizon manipulation benchmark. Following the standard protocol, models are trained on the ABC split and evaluated in the unseen D environment over 1000 rollouts. We report success rates for completing 1–5 consecutive subtasks, where evaluation terminates after the first failure, together with the average success sequence length.

As shown in Table 1, our method improves both VLM4VLA and FLOWER on CALVIN ABC→D. These gains show that directly supervising the vision encoder with inverse dynamics improves long-horizon manipulation performance across different VLA architectures. Notably, the improvement on FLOWER indicates that even a strong action-modeling baseline can benefit from better visual

Table 1: Results on CALVIN ABC→D. We report success rates over 1000 rollouts for completing 1–5 tasks in a row and the average completed sequence length. Bold numbers indicate the best results in each column. * indicates results reproduced in our environment.

| Method | Tasks completed in a row | | | | | Avg. Len. ↑ |
|------------------|--------------------------|--------------------|--------------------|--------------------|--------------------|---------------------|
| | 1 | 2 | 3 | 4 | 5 | |
| GR-1 [8] | 85.4 | 71.2 | 59.6 | 49.7 | 40.1 | 3.06 |
| UP-VLA [9] | 92.8 | 86.5 | 81.5 | 76.9 | 69.9 | 4.08 |
| RoboVLMs [37] | 98.0 | 93.6 | 85.4 | 77.8 | 70.4 | 4.25 |
| Seer [47] | 96.3 | 91.6 | 86.1 | 80.3 | 74.0 | 4.28 |
| VPP [48] | 96.5 | 90.9 | 86.6 | 82.0 | 76.9 | 4.33 |
| VLA-Adapter [40] | 99.1 | 94.6 | 88.8 | 82.8 | 76.5 | 4.42 |
| DreamVLA [11] | 98.2 | 94.6 | 89.5 | 83.4 | 78.1 | 4.44 |
| VLM4VLA* [58] | 93.4 | 85.9 | 79.7 | 75.2 | 69.2 | 4.03 |
| + Ours | 94.4 (+1.0) | 86.7 (+0.8) | 81.5 (+1.8) | 76.6 (+1.4) | 70.5 (+1.3) | 4.10 (+0.07) |
| FLOWER [39] | 99.3 | 95.9 | 90.5 | 84.8 | 77.5 | 4.54 |
| + Ours | 99.5 (+0.2) | 96.6 (+0.7) | 91.2 (+0.7) | 86.9 (+2.1) | 81.6 (+4.1) | 4.56 (+0.02) |

Table 2: Results on the SimplerEnv Bridge benchmark. We report task success rates over 24 trials for each object category and the average success rate across categories. Bold numbers indicate the best results in each column. * indicates results reproduced in our environment.

| Method | Carrot | Eggplant | Spoon | Cube | Average ↑ |
|-------------------------------|-------------|--------------------|-------------|--------------------|--------------------|
| OpenVLA [30] | 0.0 | 0.0 | 0.0 | 4.1 | 1.0 |
| RoboVLMs (pre-trained) [37] | 25.0 | 0.0 | 20.8 | 8.3 | 13.5 |
| RoboVLMs (fine-tuned) [37] | 25.0 | 58.3 | 20.8 | 12.5 | 31.3 |
| SpatialVLA (pre-trained) [33] | 20.8 | 54.2 | 12.3 | 20.8 | 27.0 |
| SpatialVLA* (fine-tuned) [33] | 12.5 | 66.6 | 25.0 | 16.7 | 30.2 |
| + Ours | 12.5 | 75.0 (+8.4) | 25.0 | 20.8 (+4.1) | 33.3 (+3.1) |

representation learning, suggesting that vision encoder supervision addresses a remaining bottleneck beyond advances in action decoding.

4.3 SimplerEnv-Bridge

We next evaluate our method on SimplerEnv (WidowX) using SpatialVLA trained on Bridge. Following the SpatialVLA evaluation protocol, we evaluate on four manipulation tasks and report final task success over 24 trials.

As shown in Table 2, our method improves SpatialVLA on SimplerEnv. These results show that inverse dynamics supervision for the vision encoder remains effective when trained on real-world robot data. The gain on a spatially structured VLA model further suggests that improving visual representation learning remains beneficial beyond standard action prediction architectures.

4.4 Frozen vision encoder evaluation

While Secs. 4.2 and 4.3 show improved policy performance, they do not directly reveal whether the vision encoder itself learns better representations. To address this, we perform frozen-encoder evaluations on LIBERO, inspired by [54], to probe how well the learned visual features support downstream behavior cloning and state prediction.

Evaluation protocol. We compare three frozen vision encoders: the original Qwen3VL-8B encoder used to initialize VLM4VLA, VLM4VLA after LIBERO-90 pretraining, and VLM4VLA + Ours after the same pretraining. For each encoder, we train only lightweight MLP heads while keeping the vision encoder fixed. We evaluate the frozen features with three probes: vision-only behavior cloning success, behavior cloning train/validation loss, and proprioceptive state prediction. Detailed training configurations are provided in Appendix A.

Table 3: Frozen-encoder behavior cloning evaluation on LIBERO. We compare the original Qwen3VL-8B vision encoder, VLM4VLA, and VLM4VLA + Ours after LIBERO-90 pretraining. We run 20 trials per task, corresponding to 200 trials per suite. Bold numbers indicate the best results in each column.

| Vision Encoder | Spatial | Object | Goal | Long | Average \uparrow |
|----------------|--------------|---------------------|---------------------|---------------------|---------------------|
| Qwen3VL-8B [4] | 49.5% | 39.5% | 43.0% | 9.5% | 35.4% |
| VLM4VLA [58] | 57.0% | 39.5% | 55.0% | 18.0% | 42.4% |
| + Ours | 57.0% | 43.5% (+4.0) | 63.0% (+8.0) | 19.5% (+1.5) | 45.8% (+3.4) |

Table 4: Frozen-encoder loss analysis on LIBERO. We report average training and validation losses for behavior cloning and proprioceptive state prediction. Lower is better, and bold numbers indicate the lowest loss in each column.

| Vision Encoder | Behavior Cloning | | State Prediction | |
|----------------|--------------------|-------------------|--------------------|-------------------|
| | Train \downarrow | Val. \downarrow | Train \downarrow | Val. \downarrow |
| Qwen3VL-8B [4] | 0.208 | 0.266 | 0.043 | 0.043 |
| VLM4VLA [58] | 0.152 | 0.262 | 0.015 | 0.018 |
| + Ours | 0.137 | 0.265 | 0.009 | 0.014 |

Behavior cloning with frozen visual features. We first evaluate the frozen vision encoder using behavior cloning (BC). We attach a lightweight MLP policy head to the frozen encoder and train a separate vision-only BC policy for each of the 40 tasks across the four LIBERO suites: Spatial, Object, Goal, and Long. For evaluation, we execute 20 rollouts per task and report the task success rate, corresponding to 200 rollouts per suite.

As shown in Table 3, Qwen3VL-8B provides the pretrained VLM encoder reference, while VLM4VLA shows the effect of robot-data pretraining from the same initialization. Our method further improves over vanilla VLM4VLA, suggesting that auxiliary inverse dynamics learning produces visual representations more useful for downstream behavior learning.

Behavior cloning loss analysis. We further analyze training and validation losses under the same frozen-encoder BC setup. This analysis measures how easily a lightweight policy can fit the action mapping from frozen visual features. If the frozen encoder suffers from state aliasing, visually similar but action-different states are represented by similar features, forcing the BC head to assign different actions to nearly indistinguishable inputs. Therefore, lower training loss indicates that the frozen features provide a less ambiguous action mapping, which is consistent with reduced state aliasing.

As shown in Figure 1 (b) and Table 4, robot-data pretraining reduces training loss compared with the original Qwen3VL-8B encoder, and our method further lowers the average training loss. The validation losses are comparable across the three encoders. These results suggest that inverse dynamics supervision makes the frozen visual features easier to fit for downstream action prediction, providing evidence consistent with reduced state aliasing in the learned representation.

Proprioceptive state prediction probe. We also probe the frozen vision encoder with proprioceptive state prediction. We train a lightweight MLP regressor on top of frozen visual features to predict robot proprioceptive states using data from all four LIBERO suites, evaluating whether the learned representations preserve robot state information observable from images.

As shown in Figure 1 (b) and Table 4, VLM4VLA reduces state prediction loss compared with the original Qwen3VL-8B encoder, and our method further reduces both training and validation losses. These results indicate that our method better preserves robot state information in the visual representation, providing additional evidence for more precise visual understanding in robotic manipulation.

4.5 Analysis

State-feature alignment. We analyze state-feature alignment to examine whether the learned visual representations become more suitable for action prediction. A representation that distinguishes different robot states can reduce state aliasing, where action-relevantly different states are mapped to

Table 5: State-feature alignment on CALVIN. We report pixel-controlled partial Spearman correlations between visual feature distances and normalized 6-DoF end-effector pose distances using 6,000 frame pairs from CALVIN validation trajectories. Higher is better, and bold numbers indicate the best results.

| Model | Mean cosine distance \uparrow | Scale difference \uparrow |
|----------------|---------------------------------|-----------------------------|
| Qwen3VL-8B [4] | 0.184 | 0.002 |
| VLM4VLA [58] | 0.489 | 0.242 |
| Ours | 0.600 | 0.309 |

Table 6: Ablation results on CALVIN ABC \rightarrow D under the same evaluation setting as Table 1. AUX denotes auxiliary inverse dynamics learning without Pseudo Time Reversal, and PTR denotes the full method with Pseudo Time Reversal. We report success rates over 1000 rollouts for completing 1–5 tasks in a row and the average completed sequence length. Bold numbers indicate the best results in each column.

| Method | 1 | 2 | 3 | 4 | 5 | Avg. Len. \uparrow |
|--------------|--------------------|--------------------|--------------------|--------------------|--------------------|----------------------|
| VLM4VLA [58] | 93.4 | 85.9 | 79.7 | 75.2 | 69.2 | 4.03 |
| + AUX | 94.3 (+0.9) | 87.1 (+1.2) | 81.1 (+1.4) | 76.3 (+1.1) | 70.2 (+1.0) | 4.09 |
| + PTR | 94.4 (+0.1) | 86.7 (-0.4) | 81.5 (+0.4) | 76.6 (+0.3) | 70.5 (+0.3) | 4.10 |

overly similar features. To measure this, we evaluate whether feature-space distances reflect robot-state distances. Specifically, we sample frame pairs from the same language-annotated trajectory segment and compute a pixel-controlled partial Spearman correlation between the visual feature distance and the normalized 6-DoF end-effector pose distance, while controlling for low-level pixel differences measured by pixel MSE. We report this correlation using two complementary feature metrics: the cosine distance between mean-pooled visual token features and the scale difference between their feature norms. Further details are provided in Appendix A.8. As shown in Figure 1 (c) and Table 5, the pretrained encoder exhibits weak alignment with robot pose changes in both cosine distance and feature scale, suggesting that features learned without robot action training do not sufficiently capture fine-grained robot-state variations. The VLM4VLA baseline improves this alignment, while adding our method further increases the correlation from 0.4886 to 0.5996 for cosine distance and from 0.2424 to 0.3094 for feature-scale difference. These results indicate that our inverse-dynamics supervision makes the visual representation more sensitive to control-relevant state changes beyond raw pixel differences, thereby reducing state aliasing.

Ablation study. We conduct an ablation study on CALVIN ABC \rightarrow D using VLM4VLA to isolate the contribution of Pseudo Time Reversal (PTR), comparing auxiliary inverse dynamics learning (AUX) with and without PTR. As shown in Table 6, auxiliary inverse dynamics already improves performance over the vanilla baseline, and adding PTR yields a further gain. This result shows that PTR provides a meaningful additional benefit beyond auxiliary inverse dynamics alone.

5 Limitations & Future Works

Our method assumes access to temporally paired observations and actions during training, which is natural for offline robot demonstrations but may be limited in online or streaming settings, even though inverse dynamics supervision can sometimes be constructed from past observations and executed actions. Extending inverse dynamics supervision to such settings remains an important future direction. PTR also relies on pseudo-reversed rather than physically exact reverse actions; future work could explore learned backward dynamics. Finally, PTR currently expands action diversity only through forward and pseudo-reversed directions, and richer transition augmentations may further improve generalization.

6 Conclusion

In this paper, we present inverse dynamics learning as an auxiliary objective for VLA vision encoder learning to mitigate state aliasing. By supervising the encoder to predict actions between current

and future observations, our method encourages visual representations that preserve fine-grained distinctions needed for low-level control and reduces state aliasing between visually similar states. We also introduce Pseudo Time Reversal (PTR) to improve generalization under limited action diversity. After training, the auxiliary head is removed, leaving the main VLA policy architecture and inference process intact. Extensive experiments across robot manipulation benchmarks demonstrate consistent performance gains across diverse VLA baselines. Beyond policy success, frozen-encoder probing and state-feature alignment analysis show that our method learns visual features that are more useful for downstream action and robot state prediction and better aligned with actual robot state changes. These results provide evidence that inverse dynamics supervision reduces state aliasing in the vision encoder, suggesting an effective direction for building more reliable VLA policies.

References

- [1] Haotian Liu, Chunyuan Li, Qingyang Wu, and Yong Jae Lee. Visual instruction tuning. In *NeurIPS*, 2023.
- [2] Siddharth Karamcheti, Suraj Nair, Ashwin Balakrishna, Percy Liang, Thomas Kollar, and Dorsa Sadigh. Prismatic VLMs: Investigating the design space of visually-conditioned language models. In *ICML*, 2024.
- [3] Lucas Beyer, Andreas Steiner, André Susano Pinto, Alexander Kolesnikov, Xiao Wang, Daniel Salz, Maxim Neumann, Ibrahim Alabdulmohsin, Michael Tschannen, Emanuele Bugliarello, Thomas Unterthiner, Daniel Keysers, Skanda Koppula, Fangyu Liu, Adam Grycner, Alexey A. Gritsenko, Neil Houlsby, Manoj Kumar, Keran Rong, Julian Eisenschlos, Rishabh Kabra, Matthias Bauer, Matko Bosnjak, Xi Chen, Matthias Minderer, Paul Voigtlaender, Ioana Bica, Ivana Balazevic, Joan Puigcerver, Pinelopi Papalampidi, Olivier J. Hénaff, Xi Xiong, Radu Soricut, Jeremiah Harmsen, and Xiaohua Zhai. PaliGemma: A versatile 3b VLM for transfer. *arXiv preprint arXiv:2407.07726*, 2024.
- [4] Qwen Team. Qwen3-VL technical report. *arXiv preprint arXiv:2511.21631*, 2025.
- [5] Boyang Zheng, Jinjin Gu, Shijun Li, and Chao Dong. LM4LV: A frozen large language model for low-level vision tasks. *arXiv preprint arXiv:2405.15734*, 2024.
- [6] Boyuan Chen, Zhuo Xu, Sean Kirmani, Brian Ichter, Dorsa Sadigh, Leonidas J. Guibas, and Fei Xia. SpatialVLM: Endowing vision-language models with spatial reasoning capabilities. In *CVPR*, 2024.
- [7] Chuan Wen, Dinesh Jayaraman, and Yang Gao. Can transformers capture spatial relations between objects? In *ICLR*, 2024.
- [8] Hongtao Wu, Ya Jing, Chilam Cheang, Guangzeng Chen, Jiafeng Xu, Xinghang Li, Minghuan Liu, Hang Li, and Tao Kong. Unleashing large-scale video generative pre-training for visual robot manipulation. In *ICLR*, 2024.
- [9] Jianke Zhang, Yanjiang Guo, Yucheng Hu, Xiaoyu Chen, Xiang Zhu, and Jianyu Chen. UP-VLA: A unified understanding and prediction model for embodied agent. In *ICML*, 2025.
- [10] Qingqing Zhao, Yao Lu, Moo Jin Kim, Zipeng Fu, Zhuoyang Zhang, Yecheng Wu, Zhaoshuo Li, Qianli Ma, Song Han, Chelsea Finn, Ankur Handa, Tsung-Yi Lin, Gordon Wetzstein, Ming-Yu Liu, and Donglai Xiang. CoT-VLA: Visual chain-of-thought reasoning for vision-language-action models. In *CVPR*, 2025.
- [11] Wenyao Zhang, Hongsi Liu, Zekun Qi, Yunnan Wang, XinQiang Yu, Jiazhao Zhang, Runpei Dong, Jiawei He, He Wang, Zhizheng Zhang, Li Yi, Wenjun Zeng, and Xin Jin. DreamVLA: A vision-language-action model dreamed with comprehensive world knowledge. In *NeurIPS*, 2025.
- [12] Yuqi Wang, Xinghang Li, Wenxuan Wang, Junbo Zhang, Yingyan Li, Yuntao Chen, Xinlong Wang, and Zhaoxiang Zhang. Unified vision-language-action model. In *ICLR*, 2026.

- [13] Dantong Niu, Yuvan Sharma, Giscard Biamby, Jerome Quenum, Yutong Bai, Baifeng Shi, Trevor Darrell, and Roei Herzig. LLARVA: vision-action instruction tuning enhances robot learning. In *CoRL*, 2024.
- [14] Jianwei Yang, Reuben Tan, Qianhui Wu, Ruijie Zheng, Baolin Peng, Yongyuan Liang, Yu Gu, Mu Cai, Seonghyeon Ye, Joel Jang, Yuquan Deng, and Jianfeng Gao. Magma: A foundation model for multimodal AI agents. In *CVPR*, 2025.
- [15] Jason Lee, Jiafei Duan, Haoquan Fang, Yuquan Deng, Boyang Li, Shuo Liu, Bohan Fang, Jieyu Zhang, Yi Ru Wang, Sangho Lee, Winson Han, Wilbert Pumacay, Angelica Wu, Rose Hendrix, Karen Farley, Eli VanderBilt, Ali Farhadi, Dieter Fox, and Ranjay Krishna. MolmoAct: Action reasoning models that can reason in space. In *CoRL Workshop on Making Sense of Data in Robotics*, 2025.
- [16] Yiye Chen, Yanan Jian, Xiaoyi Dong, Shuxin Cao, Jing Wu, Patricio A. Vela, Benjamin E. Lundell, and Dongdong Chen. VISTA: Enhancing visual conditioning via track-following preference optimization in vision-language-action models. *arXiv preprint arXiv:2602.05049*, 2026.
- [17] Yifu Yuan, Haiqin Cui, Yaoting Huang, Yibin Chen, Fei Ni, Zibin Dong, Pengyi Li, Yan Zheng, Hongyao Tang, and Jianye Hao. Embodied-r1: Reinforced embodied reasoning for general robotic manipulation. In *ICLR*, 2026.
- [18] Shaoan Wang, Jiazhao Zhang, Minghan Li, Jiahang Liu, Anqi Li, Kui Wu, Fangwei Zhong, Junzhi Yu, Zhizheng Zhang, and He Wang. TrackVLA: Embodied visual tracking in the wild. In *CoRL*, 2025.
- [19] Michal Zawalski, William Chen, Karl Pertsch, Oier Mees, Chelsea Finn, and Sergey Levine. Robotic control via embodied chain-of-thought reasoning. In *CoRL*, 2024.
- [20] Qi Sun, Pengfei Hong, Pala Tej Deep, Vernon Toh, U-Xuan Tan, Deepanway Ghosal, and Soujanya Poria. Emma-X: An embodied multimodal action model with grounded chain of thought and look-ahead spatial reasoning. In *ACL*, 2025.
- [21] Chi-Pin Huang, Yueh-Hua Wu, Min-Hung Chen, Yu-Chiang Frank Wang, and Fu-En Yang. ThinkAct: Vision-language-action reasoning via reinforced visual latent planning. In *NeurIPS*, 2025.
- [22] Jung Yeon Park and Lawson L. S. Wong. Robust imitation of a few demonstrations with a backwards model. In *NeurIPS*, 2022.
- [23] Jie-Jing Shao, Hao-Sen Shi, Lan-Zhe Guo, and Yu-Feng Li. Offline imitation learning with model-based reverse augmentation. In *KDD*, 2024.
- [24] Youguang Xing, Xu Luo, Junlin Xie, Lianli Gao, Heng Tao Shen, and Jingkuan Song. Shortcut learning in generalist robot policies: The role of dataset diversity and fragmentation. In *CoRL*, 2025.
- [25] Oier Mees, Lukás Hermann, Erick Rosete-Beas, and Wolfram Burgard. CALVIN: A benchmark for language-conditioned policy learning for long-horizon robot manipulation tasks. *IEEE Robotics Autom. Lett.*, 2022.
- [26] Xuanlin Li, Kyle Hsu, Jiayuan Gu, Oier Mees, Karl Pertsch, Homer Rich Walke, Chuyuan Fu, Ishikaa Lunawat, Isabel Sieh, Sean Kirmani, Sergey Levine, Jiajun Wu, Chelsea Finn, Hao Su, Quan Vuong, and Ted Xiao. Evaluating real-world robot manipulation policies in simulation. In *CoRL*, 2024.
- [27] Bo Liu, Yifeng Zhu, Chongkai Gao, Yihao Feng, Qiang Liu, Yuke Zhu, and Peter Stone. LIBERO: benchmarking knowledge transfer for lifelong robot learning. In *NeurIPS*, 2023.
- [28] Brianna Zitkovich, Tianhe Yu, Sichun Xu, Peng Xu, Ted Xiao, Fei Xia, Jialin Wu, Paul Wohlhart, Stefan Welker, Ayzaan Wahid, Quan Vuong, Vincent Vanhoucke, Huong T. Tran, Radu Soricut, Anikait Singh, Jaspiar Singh, Pierre Sermanet, Pannag R. Sanketi, Grecia Salazar, Michael S.

- Ryoo, Krista Reymann, Kanishka Rao, Karl Pertsch, Igor Mordatch, Henryk Michalewski, Yao Lu, Sergey Levine, Lisa Lee, Tsang-Wei Edward Lee, Isabel Leal, Yuheng Kuang, Dmitry Kalashnikov, Ryan Julian, Nikhil J. Joshi, Alex Irpan, Brian Ichter, Jasmine Hsu, Alexander Herzog, Karol Hausman, Keerthana Gopalakrishnan, Chuyuan Fu, Pete Florence, Chelsea Finn, Kumar Avinava Dubey, Danny Driess, Tianli Ding, Krzysztof Marcin Choromanski, Xi Chen, Yevgen Chebotar, Justice Carbajal, Noah Brown, Anthony Brohan, Montserrat Gonzalez Arenas, and Kehang Han. RT-2: vision-language-action models transfer web knowledge to robotic control. In *CoRL*, 2023.
- [29] Kevin Black, Noah Brown, Danny Driess, Adnan Esmail, Michael Robert Equi, Chelsea Finn, Niccolo Fusai, Lachy Groom, Karol Hausman, Brian Ichter, Szymon Jakubczak, Tim Jones, Liyiming Ke, Sergey Levine, Adrian Li-Bell, Mohith Mothukuri, Suraj Nair, Karl Pertsch, Lucy Xiaoyang Shi, Laura Smith, James Tanner, Quan Vuong, Anna Walling, Haohuan Wang, and Ury Zhilinsky. π_0 : A vision-language-action flow model for general robot control. In *RSS*, 2025.
- [30] Moo Jin Kim, Karl Pertsch, Siddharth Karamcheti, Ted Xiao, Ashwin Balakrishna, Suraj Nair, Rafael Rafailov, Ethan Paul Foster, Pannag R. Sanketi, Quan Vuong, Thomas Kollar, Benjamin Burchfiel, Russ Tedrake, Dorsa Sadigh, Sergey Levine, Percy Liang, and Chelsea Finn. OpenVLA: An open-source vision-language-action model. In *CoRL*, 2024.
- [31] Qixiu Li, Yaobo Liang, Zeyu Wang, Lin Luo, Xi Chen, Mozheng Liao, Fangyun Wei, Yu Deng, Sicheng Xu, Yizhong Zhang, Xiaofan Wang, Bei Liu, Jianlong Fu, Jianmin Bao, Dong Chen, Yuanchun Shi, Jiaolong Yang, and Baining Guo. CogACT: A foundational vision-language-action model for synergizing cognition and action in robotic manipulation. *arXiv preprint arXiv:2411.19650*, 2024.
- [32] Junjie Wen, Yichen Zhu, Minjie Zhu, Zhibin Tang, Jinming Li, Zhongyi Zhou, Xiaoyu Liu, Chaomin Shen, Yaxin Peng, and Feifei Feng. DiffusionVLA: Scaling robot foundation models via unified diffusion and autoregression. In *ICML*, 2025.
- [33] Delin Qu, Haoming Song, Qizhi Chen, Yuanqi Yao, Xinyi Ye, Jiayuan Gu, Zhigang Wang, Yan Ding, Bin Zhao, Dong Wang, and Xuelong Li. SpatialVLA: Exploring Spatial Representations for Visual-Language-Action Models. In *RSS*, 2025.
- [34] Peiyan Li, Yixiang Chen, Hongtao Wu, Xiao Ma, Xiangnan Wu, Yan Huang, Liang Wang, Tao Kong, and Tieniu Tan. BridgeVLA: Input-output alignment for efficient 3d manipulation learning with vision-language models. In *NeurIPS*, 2025.
- [35] Jiaming Liu, Hao Chen, Zhuoyang Liu, Pengju An, Renrui Zhang, Chenyang Gu, Xiaoqi Li, Ziyu Guo, Sixiang Chen, Mengzhen Liu, Chengkai Hou, Mengdi Zhao, KC alex Zhou, Pheng-Ann Heng, and Shanghang Zhang. HybridVLA: Collaborative diffusion and autoregression in a unified vision-language-action model. In *ICLR*, 2026.
- [36] Danny Driess, Jost Tobias Springenberg, Brian Ichter, Lili Yu, Adrian Li-Bell, Karl Pertsch, Allen Z. Ren, Homer Walke, Quan Vuong, Lucy Xiaoyang Shi, and Sergey Levine. Knowledge insulating vision-language-action models: Train fast, run fast, generalize better. In *NeurIPS*, 2025.
- [37] Xinghang Li, Peiyan Li, Long Qian, Minghuan Liu, Dong Wang, Jirong Liu, Bingyi Kang, Xiao Ma, Xinlong Wang, Di Guo, Tao Kong, Hanbo Zhang, and Huaping Liu. What matters in building vision–language–action models for generalist robots. *Nature Machine Intelligence*, 2026.
- [38] Moo Jin Kim, Chelsea Finn, and Percy Liang. Fine-tuning vision-language-action models: Optimizing speed and success. *arXiv preprint arXiv:2502.19645*, 2025.
- [39] Moritz Reuss, Hongyi Zhou, Marcel Rühle, Ömer Erdiñç Yağmurlu, Fabian Otto, and Rudolf Lioutikov. FLOWER: Democratizing generalist robot policies with efficient vision-language-flow models. In *CoRL*, 2025.

- [40] Yihao Wang, Pengxiang Ding, Lingxiao Li, Can Cui, Zirui Ge, Xinyang Tong, Wenxuan Song, Han Zhao, Wei Zhao, Pengxu Hou, Siteng Huang, Yifan Tang, Wenhui Wang, Ru Zhang, Jianyi Liu, and Donglin Wang. VLA-Adapter: An effective paradigm for tiny-scale vision-language-action model. In *AAAI*, 2026.
- [41] Shuai Yang, Hao Li, Bin Wang, Yilun Chen, Yang Tian, Tai Wang, Hanqing Wang, Feng Zhao, Yiyi Liao, and Jiangmiao Pang. Vision-language-action instruction tuning: From understanding to manipulation. In *ICLR*, 2026.
- [42] Kevin Black, Noah Brown, James Darpinian, Karan Dhabalia, Danny Driess, Adnan Esmail, Michael Robert Equi, Chelsea Finn, Niccolo Fusai, Manuel Y. Galliker, Dibya Ghosh, Lachy Groom, Karol Hausman, brian ichter, Szymon Jakubczak, Tim Jones, Liyiming Ke, Devin LeBlanc, Sergey Levine, Adrian Li-Bell, Mohith Mothukuri, Suraj Nair, Karl Pertsch, Allen Z. Ren, Lucy Xiaoyang Shi, Laura Smith, Jost Tobias Springenberg, Kyle Stachowicz, James Tanner, Quan Vuong, Homer Walke, Anna Walling, Haohuan Wang, Lili Yu, and Ury Zhilinsky. $\pi_{0.5}$: a vision-language-action model with open-world generalization. In *CoRL*, 2025.
- [43] Wenhui Huang, Changhe Chen, Han Qi, Chen Lv, Yilun Du, and Heng Yang. MoTVLA: A vision-language-action model with unified fast-slow reasoning. *arXiv preprint arXiv:2510.18337*, 2025.
- [44] Chi-Pin Huang, Yunze Man, Zhiding Yu, Min-Hung Chen, Jan Kautz, Yu-Chiang Frank Wang, and Fu-En Yang. Fast-ThinkAct: Efficient vision-language-action reasoning via verbalizable latent planning. *arXiv preprint arXiv:2601.09708*, 2026.
- [45] Taeyoung Kim, Jimin Lee, Myungkyu Koo, Dongyoung Kim, Kyungmin Lee, Changyeon Kim, Younggyo Seo, and Jinwoo Shin. Contrastive representation regularization for vision-language-action models. *arXiv preprint arXiv:2510.01711*, 2025.
- [46] Yilun Du, Sherry Yang, Bo Dai, Hanjun Dai, Ofir Nachum, Josh Tenenbaum, Dale Schuurmans, and Pieter Abbeel. Learning universal policies via text-guided video generation. In *NeurIPS*, 2023.
- [47] Yang Tian, Sizhe Yang, Jia Zeng, Ping Wang, Dahua Lin, Hao Dong, and Jiangmiao Pang. Predictive inverse dynamics models are scalable learners for robotic manipulation. In *ICLR*, 2025.
- [48] Yucheng Hu, Yanjiang Guo, Pengchao Wang, Xiaoyu Chen, Yen-Jen Wang, Jianke Zhang, Koushil Sreenath, Chaochao Lu, and Jianyu Chen. Video prediction policy: A generalist robot policy with predictive visual representations. In *ICML*, 2025.
- [49] Wenyao Zhang, Bozhou Zhang, Zekun Qi, Wenjun Zeng, Xin Jin, and Li Zhang. Disentangled robot learning via separate forward and inverse dynamics pretraining. In *ICLR*, 2026.
- [50] Dominik Schmidt and Minqi Jiang. Learning to act without actions. In *ICLR*, 2024.
- [51] Seonghyeon Ye, Joel Jang, Byeongguk Jeon, Se June Joo, Jianwei Yang, Baolin Peng, Ajay Mandlekar, Reuben Tan, Yu-Wei Chao, Bill Yuchen Lin, Lars Liden, Kimin Lee, Jianfeng Gao, Luke Zettlemoyer, Dieter Fox, and Minjoon Seo. Latent action pretraining from videos. In *ICLR*, 2025.
- [52] Jiange Yang, Yansong Shi, Haoyi Zhu, Mingyu Liu, Kaijing Ma, Yating Wang, Gangshan Wu, Tong He, and Limin Wang. CoMo: Learning continuous latent motion from internet videos for scalable robot learning. *arXiv preprint arXiv:2505.17006*, 2025.
- [53] Sandeep Routray, Hengkai Pan, Unnat Jain, Shikhar Bahl, and Deepak Pathak. ViPRA: Video prediction for robot actions. In *ICLR*, 2026.
- [54] David Brandfonbrener, Ofir Nachum, and Joan Bruna. Inverse dynamics pretraining learns good representations for multitask imitation. In *NeurIPS*, 2023.
- [55] Siyuan Li, Xun Wang, Rongchang Zuo, Kewu Sun, Lingfei Cui, Jishiyu Ding, Peng Liu, and Zhe Ma. Robust visual imitation learning with inverse dynamics representations. In *AAAI*, 2024.

- [56] Donghu Kim, Hojoon Lee, Kyungmin Lee, Dongyoon Hwang, and Jaegul Choo. Investigating pre-training objectives for generalization in vision-based reinforcement learning. In *ICML*, 2024.
- [57] Zichen Jeff Cui, Hengkai Pan, Aadithya Iyer, Siddhant Haldar, and Lerrel Pinto. DynaMo: In-domain dynamics pretraining for visuo-motor control. In *NeurIPS*, 2024.
- [58] Jianke Zhang, Xiaoyu Chen, Yanjiang Guo, Yucheng Hu, and Jianyu Chen. VLM4VLA: Revisiting vision-language-models in vision-language-action models. In *ICLR*, 2026.

A Implementation details

A.1 Inverse dynamics head

We implement the inverse dynamics head as a lightweight two-view MLP decoder. Let Z^{cur} and Z^{fut} denote the encoded visual token features of the current and future observations, respectively:

$$Z^{\text{cur}}, Z^{\text{fut}} \in \mathbb{R}^{B \times P \times C},$$

where B is the batch size, P is the number of visual tokens produced by the vision encoder, and C is the token feature dimension, we first compute their token-wise difference:

$$Z^{\text{diff}} = Z^{\text{fut}} - Z^{\text{cur}}.$$

We then concatenate the current, future, and difference features along the channel dimension:

$$Z^{\text{cat}} = [Z^{\text{cur}}, Z^{\text{fut}}, Z^{\text{diff}}] \in \mathbb{R}^{B \times P \times 3C}.$$

Each concatenated token is processed independently by a patch-wise fusion MLP, which projects the feature dimension from $3C$ to a decoder dimension. The resulting fused token features are flattened across the token dimension and passed to an action MLP, which predicts an action chunk:

$$\bar{a}_{t:t+H} = h_{\psi}(Z^{\text{cat}}) \in \mathbb{R}^{B \times H \times d_a},$$

where H denotes the action chunk length chosen for each benchmark and $d_a = 7$ denotes the action dimension.

For observations with multiple input types or camera views, we apply the inverse dynamics head independently to each type. For each input type, we encode the observations at time steps t and $t+k$, compute the corresponding inverse dynamics prediction, and evaluate the auxiliary loss using the same action target. The final inverse dynamics loss is averaged across all available input types. The batch size, number of visual tokens, decoder dimension, action chunk length, and other benchmark-specific hyperparameters are reported in the corresponding implementation tables. The inverse dynamics head is used only during training and removed at inference time.

A.2 Probing MLP heads

For frozen-encoder evaluation, we attach lightweight MLP probing heads on top of the frozen vision encoder. The vision encoder is kept fixed throughout all probing experiments, and only the newly added MLP head is trained. Both behavior cloning and proprioceptive state prediction use the same probing architecture, differing only in the output dimension and training loss.

Given an input observation, the frozen vision encoder produces visual tokens

$$Z \in \mathbb{R}^{B \times P \times C},$$

where B is the batch size, P is the number of visual tokens, and C is the token feature dimension. Each token is first projected independently by a token projection MLP:

$$Z^{\text{proj}} = \text{GELU}(\text{Linear}(Z)), \quad Z^{\text{proj}} \in \mathbb{R}^{B \times P \times D_{\text{proj}}}.$$

The projected tokens are then flattened into a single feature vector and passed to a three-layer MLP head:

$$u = \text{Flatten}(Z^{\text{proj}}),$$

Table 7: Implementation details for FLOWER on CALVIN ABC→D.

| Parameter | Value |
|--|--|
| VLM backbone | Florence-2-large |
| Pretrained checkpoint | FLOWER pretrained checkpoint |
| Input views | Static view + wrist view |
| Training steps | 40K |
| Batch size | 32 |
| Optimizer | AdamW |
| Learning rate | 2×10^{-5} |
| Learning rate schedule | Three-phase schedule (0.05, 0.1, 0.85) |
| Weight decay | 0.05 |
| Action dimension | 7 |
| Action chunk length | 10 |
| Flow sampling steps | 4 |
| DiT dimension / layers / heads | 1024 / 18 / 16 |
| Token dropout | 0.1 |
| Auxiliary loss weight λ_{inv} | 0.3 |
| Gripper loss weight (in auxiliary) λ_g | 0.01 |
| PTR probability p_{rev} | 0.5 |
| Inverse dynamics decoder dimension | 1024 |
| Checkpoint used for evaluation | Final checkpoint |

$$\hat{y} = f_{\theta}(u).$$

The MLP head consists of two hidden layers with GELU activations and dropout, followed by a linear output layer:

$$f_{\theta} : PD_{\text{proj}} \rightarrow 2D_{\text{hidden}} \rightarrow D_{\text{hidden}} \rightarrow d_{\text{out}}.$$

For the behavior cloning probe, the output is reshaped into an action chunk,

$$\hat{a}_{t:t+H_{\text{BC}}} \in \mathbb{R}^{B \times H_{\text{BC}} \times d_a},$$

where H_{BC} is the prediction horizon and $d_a = 7$ is the action dimension. For the proprioceptive state prediction probe, the output dimension is set to the target proprioceptive state dimension d_s . In all probing experiments, we use the static RGB view only. We set $D_{\text{proj}} = 256$, $D_{\text{hidden}} = 512$.

A.3 CALVIN ABC→D implementation details

CALVIN ABC→D is a language-conditioned long-horizon manipulation benchmark that evaluates generalization to an unseen environment. Models are trained on demonstrations from environments A, B, and C, and evaluated in environment D. During evaluation, a policy is required to execute a sequence of tabletop manipulation subtasks from visual observations and language instructions. Following the standard protocol, we evaluate each model over 1000 rollouts and report the success rates for completing 1, 2, 3, 4, and 5 consecutive subtasks, as well as the average number of successfully completed subtasks.

For each baseline, we keep the original training pipeline unchanged and add only our auxiliary inverse dynamics loss and PTR. We use the same training budget and evaluation protocol for each baseline and its +Ours variant. Model-specific training details are provided below.

A.3.1 FLOWER

Except for the hyperparameters related to our auxiliary objective, we keep the FLOWER training configuration identical to the default hyperparameters released in the official implementation and reported in the original paper. Since our reproduced vanilla FLOWER model did not reach performance comparable to the reported result, we report the publicly available number from the original paper for the vanilla baseline. For our +Ours variant, we train with the same default configuration while adding only auxiliary inverse dynamics learning and PTR. Detailed implementation settings are provided in Table 7.

Table 8: Implementation details for VLM4VLA on CALVIN ABC→D.

| Parameter | Value |
|--|----------------------|
| VLM backbone | Qwen3-VL-8B-Instruct |
| Training steps | 30K |
| Batch size | 128 |
| Optimizer | Adam |
| Learning rate | 2×10^{-5} |
| Weight decay | 0 |
| Warmup epochs | 0.25 |
| Input views | Static view |
| Action dimension | 7 |
| Action chunk length | 10 |
| Auxiliary loss weight λ_{inv} | 0.1 |
| Gripper loss weight (in auxiliary) λ_g | 0.01 |
| PTR probability p_{rev} | 0.5 |
| Inverse dynamics decoder dimension | 1024 |
| Checkpoint used for evaluation | Final checkpoint |

The original FLOWER evaluation protocol reports the best checkpoint selected by evaluating every epoch after epoch 19 up to 40K training steps. Since such checkpoint selection can introduce benchmark overfitting, we instead evaluate our +Ours model using the final checkpoint only. Training the +Ours variant takes approximately 4 hours on 4 NVIDIA H100 GPUs.

A.3.2 VLM4VLA

For VLM4VLA on CALVIN ABC→D, we follow the released configuration as closely as possible and keep the same hyperparameters for the vanilla baseline and its +Ours variant, except for the auxiliary inverse dynamics objective and PTR. The model is built on Qwen3-VL-8B-Instruct and uses the static camera view as input. Following the original paper, we evaluate both models at the 30K checkpoint. Detailed implementation settings are provided in Table 8. Training each VLM4VLA model on CALVIN takes approximately 20 hours on 8 NVIDIA H100 GPUs.

A.4 Bridge / SimplerEnv implementation details

SimplerEnv is a real-to-sim benchmark that evaluates policies trained on real-world robot data in simulated environments. It provides evaluation settings based on different data sources, including Google Robot and WidowX Bridge. Following prior VLA evaluations, we focus on the WidowX Bridge setting, which is based on the Bridge dataset.

We use SpatialVLA as the main baseline for SimplerEnv. We initialize from the released SpatialVLA pretrained checkpoint, finetune the model on Bridge, and evaluate it on four WidowX manipulation tasks: putting a spoon on a towel, putting a carrot on a plate, stacking a green block on a yellow block, and putting an eggplant into a yellow basket. For each task, we run 24 trials with randomized initializations and report the final task success rate. Detailed implementation settings are provided in Table 9.

Except for the auxiliary inverse dynamics objective and PTR used in our +Ours variant, we keep all hyperparameters identical to the official code. Since the exact training steps and checkpoint selection protocol are not specified in the official release, we train SpatialVLA for 30K steps, matching the VLM4VLA training budget used in our CALVIN experiments, and evaluate the final checkpoint. For comparison, the OpenVLA and RoboVLMs results in Table 2 are taken from [33]. We also re-evaluate the publicly released SpatialVLA pretrained checkpoint under the same SimplerEnv evaluation protocol. Training each SpatialVLA finetuning run takes approximately 16 hours on 4 NVIDIA B200 GPUs.

Table 9: Implementation details for SpatialVLA on Bridge / SimplerEnv.

| Parameter | Value |
|--|----------------------------------|
| VLM backbone | PaliGemma2 |
| Pretrained checkpoint | SpatialVLA pretrained checkpoint |
| Training steps | 30K |
| Batch size | 256 |
| Optimizer | AdamW |
| Learning rate | 2×10^{-5} |
| Weight decay | 0 |
| Warmup ratio | 0.005 |
| Input views | Static view |
| Action dimension | 7 |
| Action chunk length | 4 |
| Auxiliary loss weight λ_{inv} | 0.2 |
| Gripper loss weight (in auxiliary) λ_g | 0.01 |
| PTR probability p_{rev} | 0.5 |
| Inverse dynamics decoder dimension | 512 |
| Checkpoint used for evaluation | Final checkpoint |
| Execution steps | 1 |

Table 10: Implementation details for LIBERO-90 pretraining.

| Parameter | Value |
|---------------------------------------|----------------------|
| VLM backbone | Qwen3-VL-8B-Instruct |
| Training epochs | 1 |
| Batch size | 256 |
| Optimizer | Adam |
| Learning rate | 2×10^{-5} |
| Weight decay | 0 |
| Warmup epochs | 0.25 |
| Input views | Static view |
| Action dimension | 7 |
| Action chunk length | 4 |
| Auxiliary loss weight λ_{inv} | 0.1 |
| Gripper loss weight λ_g | 0.01 |
| PTR probability p_{rev} | 0.5 |
| Inverse dynamics decoder dimension | 1024 |
| Checkpoint used for evaluation | Final checkpoint |

A.5 LIBERO-90 pretraining

For LIBERO-90 pretraining, we use VLM4VLA with Qwen3-VL-8B-Instruct as the backbone and train on LIBERO-90 for one epoch. Except for the auxiliary inverse dynamics objective and PTR, we keep the same hyperparameters for the vanilla baseline and its +Ours variant. Both models are trained with the static camera view and evaluated using the final checkpoint for the frozen-encoder analyses. Detailed implementation settings are provided in Table 10. Training each LIBERO-90 pretraining model takes approximately 12 hours on 8 NVIDIA H100 GPUs.

A.6 Behavior cloning probe

For the behavior cloning probe, we freeze the vision encoder pretrained on LIBERO-90 and train only a lightweight MLP policy head. The probe uses visual features from the static RGB view and predicts a 4-step action chunk with 7-dimensional actions. The policy head is trained with an ℓ_1 loss on the motion offsets and a binary cross-entropy loss on the gripper action, with the gripper loss weighted by $\lambda_g = 0.01$. Detailed implementation settings are provided in Table 11.

Table 11: Implementation details for the behavior cloning probe.

| Parameter | Value |
|---------------------------------|--|
| Input views | Static view |
| Token projection dimension | 256 |
| MLP hidden dimension | 512 |
| Action dimension | 7 |
| Action chunk length | 4 |
| Output shape | $B \times (4 \times 7)$ |
| Loss | $\ell_1 + \text{BCE}$ |
| Gripper loss weight λ_g | 0.01 |
| Training loss reporting | Average over 1K steps |
| Validation loss reporting | Average of validation losses every 100 steps |
| Optimizer | Adam |
| Learning rate | 2×10^{-4} |
| Batch size | 64 |
| Training steps | 1K |
| Evaluation tasks | 40 tasks across LIBERO-Spatial, Object, Goal, and Long |
| Evaluation rollouts | 20 per task |
| Checkpoint used for evaluation | Final checkpoint |

Table 12: Implementation details for the proprioceptive state prediction probe.

| Parameter | Value |
|----------------------------|---|
| Input views | Static view |
| Token projection dimension | 256 |
| MLP hidden dimension | 512 |
| Target dimension | 8 |
| Target state | 3D EEF position + 3D axis-angle orientation + 2D gripper qpos |
| Loss | ℓ_1 |
| Optimizer | Adam |
| Learning rate | 2×10^{-4} |
| Batch size | 256 |
| Training epochs | 1 |
| Training loss reporting | Recorded at every training step |
| Validation loss reporting | Evaluated every 100 steps |

We train a separate behavior cloning probe for each of the 40 tasks across LIBERO-Spatial, Object, Goal, and Long. For each task, we use 10% of the demonstrations as the validation split. Each probe is trained for 1K steps with Adam using a learning rate of 2×10^{-4} and batch size 64. For the loss analysis, we report the average training loss over the full 1K training steps and the average validation loss computed from evaluations performed every 100 steps. For rollout evaluation, we use the final checkpoint and execute 20 rollouts per task. Training each behavior cloning probe takes approximately 1 hour on a single NVIDIA RTX 3090 GPU.

A.7 Proprioceptive state prediction probe

For the proprioceptive state prediction probe, we freeze the vision encoder pretrained on LIBERO-90 and train only a lightweight MLP regression head. The probe uses visual features from the static RGB view and predicts an 8-dimensional proprioceptive state. The target state consists of the 3D end-effector position, 3D axis-angle orientation, and 2D gripper qpos. We train the probe with an ℓ_1 regression loss. Detailed implementation settings are provided in Table 12.

This probe evaluates whether the frozen visual representations preserve robot state information that is observable from the image. Lower prediction loss indicates that the learned visual features encode more precise information about the robot configuration, complementing the behavior cloning

evaluation. Training the proprioceptive state prediction probe takes approximately 3 hours on a single NVIDIA RTX 3090 GPU.

A.8 State-feature alignment analysis

We evaluate whether visual feature distances preserve robot pose geometry after accounting for low-level image differences. The analysis uses language-annotated CALVIN validation trajectories. We first collect all frames that belong to language annotation intervals, resulting in 64,793 annotated validation records. Frame pairs are sampled only within the same language-annotated trajectory segment, so the two frames share the same instruction and high-level task context while the robot state varies. We use temporal gaps $\{1, 2, 4, 8, 16, 32\}$ and uniformly sample 1,000 pairs for each gap, yielding 6,000 frame pairs in total.

For each frame i , we use the 6-DoF end-effector pose s_i , corresponding to the first six dimensions of `robot_obs`. Let $\sigma \in \mathbb{R}^6$ denote the per-dimension standard deviation of these six pose dimensions over all annotated validation records. The target pose distance for a pair (i, j) is

$$d_{\text{pose}}(i, j) = \left\| \frac{s_i - s_j}{\sigma} \right\|_2. \quad (1)$$

For visual features, we extract spatial visual tokens from the selected vision encoder layer. The main analysis uses layer 24. We evaluate two types of feature distance: cosine distance, which measures directional feature change, and scale distance, which measures change in feature magnitude. Let h_i^k and h_j^k be the visual tokens at spatial position k , and let $\bar{h}_i = \frac{1}{K} \sum_k h_i^k$ be the mean-pooled visual feature. The pooled cosine and pooled scale distances are defined as

$$d_{\text{cos}}(i, j) = 1 - \frac{\langle \bar{h}_i, \bar{h}_j \rangle}{\|\bar{h}_i\|_2 \|\bar{h}_j\|_2}, \quad (2)$$

$$d_{\text{scale}}(i, j) = \left| \|\bar{h}_i\|_2 - \|\bar{h}_j\|_2 \right|. \quad (3)$$

To remove the effect of low-level image change, we compute a pixel-controlled partial Spearman correlation. For each pair, d_{pix} is computed as `pixel_mse` from downsampled grayscale image thumbnails. We rank-transform feature distance, pose distance, and d_{pix} . Ranked feature distance and ranked pose distance are then separately residualized against ranked d_{pix} , and the final score is the Pearson correlation between the two residual vectors:

$$\rho_{\text{partial}} = \text{corr}(\text{resid}(\text{rank}(d_{\text{feat}}), \text{rank}(d_{\text{pix}})), \text{resid}(\text{rank}(d_{\text{pose}}), \text{rank}(d_{\text{pix}}))). \quad (4)$$

This score measures whether feature distance tracks 6-DoF end-effector pose change beyond what can be explained by raw pixel-level image difference.

B Qualitative results

Figure 3 shows qualitative examples from CALVIN ABC→D and LIBERO. Each row visualizes six representative frames from a rollout. The examples illustrate that our method leads to more precise behavior compared to the vanilla VLM4VLA baseline.

In the CALVIN stack-block task, the vanilla VLM4VLA policy moves the red block toward the blue block but lowers the end-effector and releases the block before it is sufficiently aligned with the target, resulting in failure. In contrast, our method moves the red block accurately above the blue block and successfully places it on the target block.

In the LIBERO-Object task, we evaluate the frozen-encoder BC probe on the instruction "pick up the black bowl from table center and place it on the plate." The vanilla encoder-based policy moves only coarsely toward the black bowl and lowers the gripper without accurately reaching the grasp point, causing the policy to miss the object before moving toward the plate. In contrast, the policy trained on our encoder moves directly to the correct grasp region, successfully picks up the bowl, and transfers it to the target plate.

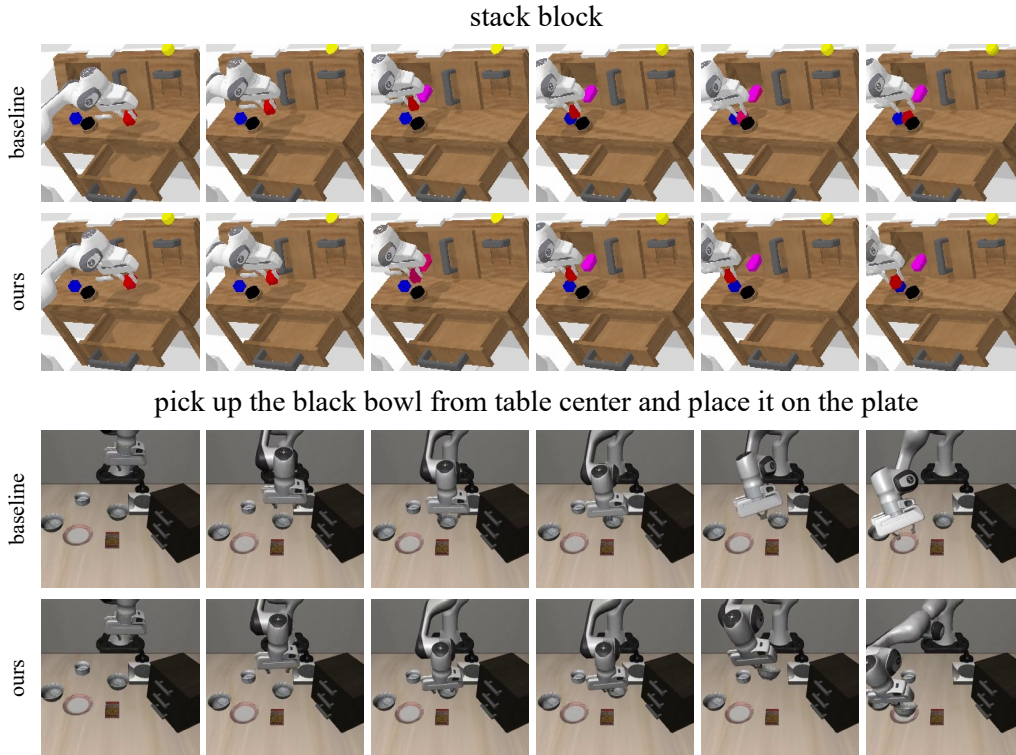


Figure 3: Qualitative results on CALVIN ABC→D and LIBERO. Each rollout is shown with six representative frames. **Top:** In the CALVIN stack-block task, the vanilla VLM4VLA policy releases the red block before it is properly aligned above the blue block, while our method accurately places the red block on the target. **Bottom:** In the LIBERO-Object task, the vanilla frozen-encoder BC policy approaches the black bowl imprecisely and fails to grasp it, whereas our method moves to the correct grasp region, picks up the bowl, and places it on the plate.

C Broader impacts

Our work aims to improve visual representation learning for vision-language-action (VLA) models in robot manipulation. A potential positive impact is that stronger and more reliable visual representations may improve the robustness and generalization of robot policies, which could benefit assistive robotics, household automation, and industrial manipulation systems. Because our method is plug-and-play and uses existing observation-action data, it may also lower the cost of improving VLA models without requiring additional annotations.

At the same time, improved robot manipulation policies may raise safety and misuse concerns if deployed without appropriate safeguards. More capable VLA policies could be used in settings where robots interact with people, fragile objects, or safety-critical environments, and failures caused by distribution shift, incorrect language instructions, or visual ambiguity could lead to unintended physical actions. The method could also improve manipulation capabilities in applications that require careful access control. We therefore emphasize that deployment should include task-specific safety constraints, human oversight, controlled evaluation under distribution shifts, and appropriate restrictions on use in safety-critical or potentially harmful settings.

D Licenses for existing assets

We use publicly available datasets, benchmarks, pretrained models, and baseline implementations only for research purposes, following their respective licenses and terms of use. We cite the original papers and repositories for all assets used in our experiments. Table 13 summarizes the main assets used in this work.

Table 13: Existing assets used in this work.

| Asset | Type | Usage in this work | License / terms |
|------------------------|--|---|---|
| CALVIN | Benchmark / simulator / Dataset | CALVIN ABC→D evaluation | MIT License, Copyright (c) 2021 Oier Mees |
| SimplerEnv | Benchmark / simulator | WidowX simulation evaluation | MIT License, Copyright (c) 2024 simpler-env |
| BridgeData V2 / Bridge | Dataset | Training data for SimplerEnv baselines | Creative Commons Attribution 4.0 International (CC BY 4.0) |
| LIBERO / LIBERO-90 | Benchmark / dataset | Frozen-encoder evaluation and pretraining | MIT License, Copyright (c) 2023 Lifelong Robot Learning |
| Qwen3-VL-8B-Instruct | Pretrained model | VLM4VLA backbone for CALVIN and LIBERO | Apache License 2.0 |
| Qwen3-VL-4B-Instruct | Pretrained model | VLM4VLA backbone for SimplerEnv | Apache License 2.0 |
| VLM4VLA | Baseline implementation | CALVIN, and LIBERO experiments | Not explicitly specified in the official repository |
| FLOWER | Baseline implementation / Pretrained model | CALVIN baseline and +Ours experiments | MIT License, Copyright (c) 2025 Moritz Reuss |
| SpatialVLA | Baseline implementation / Pretrained model | SimplerEnv baseline and +Ours experiments | MIT License; third-party code/models subject to respective licenses |